Article

Acceleration of daily land temperature extremes and correlations with surface energy fluxes

Check for updates

Chris Huntingford [1] ✉, Peter M. Cox [2,3], Paul D. L. Ritchie [2,3], Joseph J. Clarke [2], Isobel M. Parry [2] & Mark S. Williamson [2,3]

Assessment of climate reanalysis data for land (ECMWF Re-Analysis v5; ERA5-Land) covering the last seven decades reveals regions where extreme daily mean temperatures are rising faster than the average rate of temperature rise of the 6 months of highest background warmth. However, such extreme temperature acceleration is very heterogeneous, occurring only in some places including regions of Europe, the western part of North America, parts of southeast Asia and much of South America. An ensemble average of Earth System Models (ESMs) over the same period also shows acceleration across land areas, but this enhancement is much more spatially uniform in the models than it is for ERA5-Land. Examination of projections from now to the end of the 21st Century, with ESMs driven by the highest emissions Shared Socio-economic Pathway scenario (SSP585) of future changes to atmospheric greenhouse gases, also reveals larger warming during extreme days for most land areas. The increase in high-temperature extremes is driven by different processes depending on location. In northern mid-latitudes, a key driver is often a decrease in the evaporative fraction of the available energy, consistent with soil drying. By contrast, the acceleration of high-temperature extremes in tropical Africa is primarily due to increased available energy. These two drivers combine via the surface energy balance to equal the sensible heat flux, which we find is often strongly correlated with the areas where the acceleration of high-temperature extremes is largest.

As the planet warms due to rising atmospheric Greenhouse Gases (GHGs), society may be impacted the most by the altered frequency of extreme weather events. The expectation of more future regular higher-intensity extreme temperature events is widely accepted (e.g., ref. [1]), including for a climate stabilised at key thresholds such as two degrees of global warming above pre-industrial levels[2]. Concerns over more regular and intense temperature extremes are reflected by their specific mention in the Summary for Policymakers (Ref. [3], Fig. SPM.6, top two panels). Fig. SPM.6 of ref. [3] shows that even for global warming of 1.5 °C since pre-industrial times, the 1-in-10-year extreme temperature event over land would become roughly four times more likely, and extreme temperature intensity would rise by nearly 2.0 °C. Some of these higher-intensity findings may be due to background land temperatures rising faster than global mean temperatures (Ref. [4], Fig. 3). However, there is also evidence that very high-temperature events are starting to happen more frequently than expected when based solely on background temperature changes. Known places of amplified warming include tropical land[5] and Europe[6,7]. Analysis of daily temperature reveals that the upper tail of their distribution is stretching for many places as atmospheric GHGs rise. Previous studies have illustrated such distribution stretching for critical parts of the world and attribute these changes to adjusted soil moisture levels affecting land-atmosphere interactions that subsequently modulate temperature levels[8]. Hence, the distribution of temperature extremes may not be static except for an offset of local background warming, and instead change shape. However, other analyses[9] suggest that the form of temperature extremes is broadly a time-invariant distribution except for an offset of background global warming changes.

Understanding the expected changes to the statistical distribution of high temperatures is particularly important for impact planning, especially as they may occur over major areas of high population[10]. A tight relationship exists between heatwaves and excess mortality, e.g.,

[1]UK Centre for Ecology and Hydrology, Wallingford, Oxfordshire OX10 8BB, UK. [2]Department of Mathematics and Statistics, Faculty of Environment, Science and Economy, University of Exeter, Exeter, Devon EX4 4QF, UK. [3]Global Systems Institute, University of Exeter, Devon Exeter EX4 4QE, UK. ✉e-mail: chg@ceh.ac.uk

refs. 11–14, and concerns exist about high-temperature implications for food security[15,16]. Altered temperature extremes may additionally affect net land-atmosphere carbon dioxide (CO_2) exchanges and eventually decrease terrestrial carbon stocks[17], with implications for emissions trajectories designed to keep global warming below key thresholds such as two degrees. Such temperature-induced changes to CO_2 fluxes are strongly linked to region[18]. More frequent high-temperature weather events will raise the likelihood of "fire weather"[19], and more fires risk altering land biome composition[20]. A review of research on extreme high-temperature events[21] provides detailed information on their expected impacts.

Earth System Models (ESMs) (Methods) are designed to predict changes in the statistics of near-surface meteorology at different locations and in response to rises in atmospheric GHGs. As observed in the measurement record, all ESMs predict raised global mean temperatures as GHGs rise, with the latest IPCC report[22] stating, "it is unequivocal that human influence has warmed the atmosphere, ocean and land since pre-industrial times". ESMs also estimate changes on different timescales, including sub-monthly, providing outputs of daily temperature, which is our focus in understanding their changing extremes. To support the understanding of the recent past, data- and model-led reanalysis products are also available, providing high-resolution (in space and time) hindcasts covering recent decades. One such product is the 5th version of the European ReAnalysis (ERA5) product and the enhanced component over land, ERA5-Land (Methods).

Many researchers suggest that positive feedbacks accelerate temperature extremes away from mean warming, likely due to land-atmosphere feedbacks[23]. The two-way coupling between the land and atmosphere is complex, and during heatwaves is frequently associated with high soil moisture stress. Drier soils, due to the increasing likelihood of arid conditions[24], may feedback on high temperatures[25,26] and dry soils further[27,28]. Others suggest that such feedbacks modulate temperature distribution shape[8]. That analysis is extended to untangle soil moisture impacts on near-surface meteorological changes, including temperature[29]. Others establish the specific role of drier soils impacting high temperature extremes, including for Europe (e.g., refs. 30,31, parts of Africa[32], India[33] and China[34]). A further complication is inter-seasonal couplings where summer soil moisture may be lower due to higher spring evaporative losses caused by climate-induced earlier vegetation greening[35]. Well-designed ESMs should simulate such couplings and their evolution as GHGs rise.

Our focus is on hotter months, which we define as the 6 months (which are not necessarily consecutive) having the highest background temperatures at any location. The set of 6 months is invariant in time, based on the initial years of simulations or data (calculations in Methods and Supplementary Notes), and referred to henceforth as the "warmest half-year months". We use outputs from ESMs forced with the SSP585 GHG concentration pathway[36–38], which is a high emissions future. SSP585 is selected as most available ESMs have been forced with this scenario and it provides clearer signals of investigated changes while recognising that a general aim of society is to constrain GHG rise to lower levels. We calculate the warming rate during the warmest half-year months (K decade^{-1}) and a second warming rate of the top 10% of hottest days in such 6 months. If this second rate of warming is faster, we refer to this as an acceleration of extreme temperature events away from background warming of the warmest half-year months. In general, we expect to see high-temperature extremes when there is either a lot of available energy (A) warming the surface (e.g., cloud-free skies in summer) and/or when surface water is limited so that evaporative cooling of the surface is reduced (e.g., when soils are dry). We can approximate available energy as $A = H + \lambda E$ where H is surface sensible heat to the atmosphere and λE is evaporative loss from the land surface. We define Evaporative Fraction (EF) as the fraction of surface sensible heat plus latent heat that is evaporation i.e., $\lambda E/(H + \lambda E)$. The combined impact of changes in A and EF is numerically equal to upward sensible heat, noting $H = A \times (1\text{-EF})$. We, therefore, test for links between extreme temperature acceleration and trends in each of EF, H and A (latter as $H + \lambda E$).

Results

Analysis at a single location (Paris)

We first consider simulated extreme two-metre temperature changes for a single illustrative location of Paris, France, based on 32 ESMs (Supplementary Table 1) in the CMIP6 ensemble[39] (Fig. 1 and Supplementary Fig. 1). We use a single projection from each ESM and corresponding to a future GHG trajectory matching the SSP585 scenario[36,37]. We include ESMs that also provide H and λE land-atmosphere fluxes as diagnostics. For all ESMs, the modelled mean of the (six) warmest half-year month temperatures (red continuous lines) broadly increase, especially in the recent past and through to towards the end of the 21st Century (Fig. 1). Notable is that for most ESMs, the hottest 10% of days during the six warmest half-year months increase faster (red dashed lines), suggesting that there is currently an acceleration in high-temperature extreme events for Paris, which will continue as GHG rise further. We also show that most ESMs estimate that the EF during the six warmest half-year months will decrease at the Paris location (blue continuous lines). Hence, as climate changes, a larger fraction of available energy becomes sensible (i.e., thermal) upward heat, H. For simulations applicable to Paris, a substantial fraction of ESMs estimate this decrease in EF to be more exaggerated during the hottest days (blue dashed lines). However, as most ESMs only save monthly values of H and λE, this latter EF value is only the monthly mean value recorded on the day of any daily temperature extreme. While ESMs have substantial agreement, they differ in the magnitude of projected changes for the Paris region (Fig. 1).

Global analysis for the historical period since the year 1950

We expand our analysis to land locations worldwide. However, before assessing any further ESM-based evidence of future differential rates of background warming and extremes, we first focus on the recent past. Restricting to this period allows a comparison of ESM projections against a climate reanalysis product, which is highly data-derived, fusing available meteorological measurements with simulations similar to weather forecasts. We utilise the ERA5-Land reanalysis outputs[40].

We derive trends for land points from the ERA5-Land data for the years 1950–2021 inclusive. Such trends are again of the warmest half-year months and the warmest 10% of days within those 6 months. Due to the shorter period of analysis, to retain years, values contributing to the trend are for each year (rather than 41-year running means). We then calculate the ratio of these two trends as the 10% extreme trend values divided by those corresponding to the mean of the full 6-months i.e., warmest half-year months. This ratio is our primary statistic, first referred to in the Introduction, and values greater than unity are for faster warming ("acceleration") of extreme days. We present a map of this statistic (Fig. 2a) on the native grid of ERA5-Land covering a latitudinal range of −60°S to 75°N. Of note are the high levels of extreme warming acceleration for most of Europe, parts of North America, southeast Asia and Australia and much of South America. Many of these locations mirror findings by similar authors, e.g., for Europe[6,7] and South America[5].

Some high northern latitudes, and especially much of Russia (Fig. 2a), are associated with ratios less than unity, and so the temperatures of extreme hot days are warming less than the background warmest half-year month levels. Under changing climatic conditions, earlier seasonal permafrost melting may increase latent heat fluxes (e.g., ref. 41), resulting in additional evaporative cooling. In general, in recent historical data and as represented in the ERA5-Land product, there is very substantial geographical heterogeneity across the globe in the magnitude or even presence of extreme temperature acceleration (Fig. 2a). After removing a small number of outliers, the areally weighted spatial average of Fig. 2a is 1.012.

We then analyse the geographical variation in extreme acceleration in the same 32 ESMs used for the analysis at the Paris location by mapping them onto a common 2.5° × 2.5° grid. For the midpoint of these coarse gridboxes, we locate the nearest native gridbox of each ESM. An ESM is used
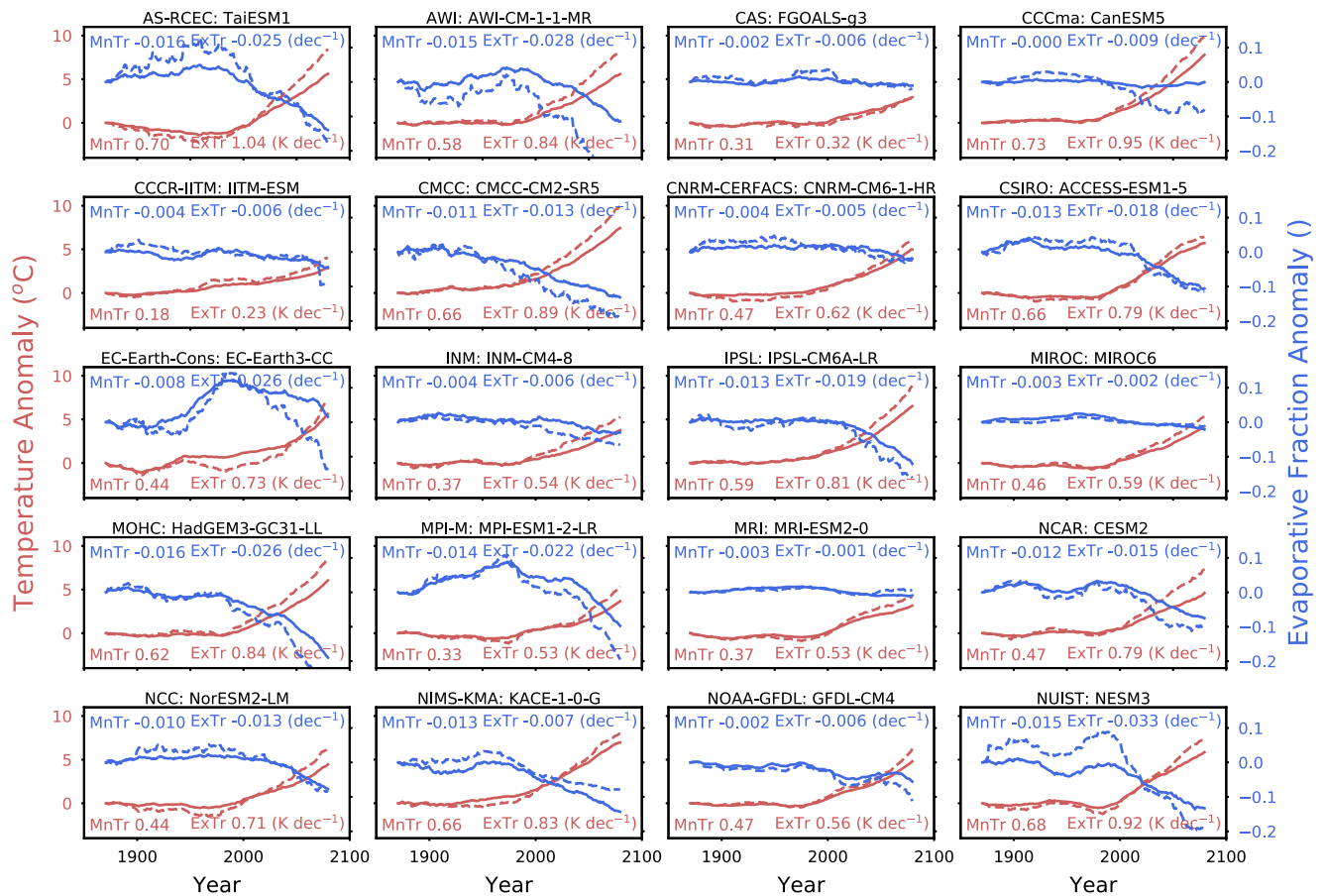
Fig. 1 | Anomalies in warmest half-year month temperatures and evaporative fraction, simulated for the Paris region. Shown are timeseries for 20 ESMs from the CMIP6 ensemble (panel titles are research centre and ESM names; centre "EC-Earth-Consortium" as "EC-Earth-Cons"). We use 32 ESMs, but where a climate modelling centre submits two or more models to the CMIP6 database, we select one for presentation (Supplementary Fig. 1 shows all 32 ESMs). Calculations for historical GHG concentrations and future projections correspond to the SSP585 GHG scenario. All values are for the period of warmest half-year months, defined as a fixed mask of the warmest 6 months of monthly means during 1850–1890 inclusive. For a moving window of 41 years and centred on the years 1870–2079 inclusive, the red continuous curves are running means of daily two-metre temperatures during the

warmest half-year months, expressed as anomalies (°C or K) relative to the first 41-year period. Red dashed curves are the top 10% of warmest days during the same 6 months, also as anomalies. The warmest days are defined as the top 10% of hottest days in 41-year periods of the warmest half-year months. Blue continuous curves are the 41-year moving mean changes in EF during the same 6 months. Most ESMs provide only monthly values of H and λE, so for days in the warmest 10%, the related monthly energy fluxes are recorded to estimate EF on extreme days (blue dashed curves). Linear trends, in sub-period 1980–2079 inclusive, are annotations for temperature (average "MnTr" changes and extreme "ExTr" changes; K decade⁻¹) at panel bases and EF trend values at panel tops (decade⁻¹). ESM values use diagnostics of the native gridbox containing the Paris latitude and longitude.

at that location if 95% of that native gridbox consists of land. A common gridbox point (i.e., on the 2.5° × 2.5° mesh) is retained for analysis if at least 30 of 32 ESMs satisfy this 95% threshold. To compare with ERA5-Land data, we derive our ratio of trends statistic for each ESM in the annual values (i.e., with no running mean smoothing) for years 1950–2021. We present the inter-ESM means of the ratio of temperature trends in Fig. 2b. While there are locations of common changes between ERA5-Land and the mean of ESMs (Fig. 2a versus Fig. 2b), the latter has far more spatial smoothness. Notably, the mean of the ESMs estimates for the historical period (Fig. 2b) have values greater than unity almost everywhere except for some northern latitude locations and an acceleration of extremes. The areally-weighted spatial average of Fig. 2b is an overall acceleration of 1.196. The areally-weighted spatial averages of the individual ESMs are given in Supplementary Table 1, and those values have an inter-ESM standard deviation of 0.199. Most ESMs, therefore, project a higher spatially averaged acceleration for the recent past than for ERA5-Land (individual values in Supplementary Table 1 compared to the value of 1.012 for ERA5-Land).

We now perform a global search to see if extreme temperature acceleration is associated with declines in background EF. Local EF trends are calculated for the mean of the six warmest half-year months and the years 1950 to 2021. We show these trends for ERA5-Land (Fig. 2c) and their mean

trend value across ESMs (Fig. 2d). Visually, there is little connection between any faster extreme temperature warming and EF for the ERA5 data, confirmed by a low r correlation value (Fig. 2a versus Fig. 2c; $r = 0.012$ with $p < 0.05$ although the very large number of points may generate the 95% statistical significance). When instead considering trends in EF on the days of extreme temperature events (Supplementary Fig. 2c), we find the correlation to be slightly negative ($r = -0.006$). For the ESMs there is some connection to EF, depending on region (e.g., South America) (Fig. 2b versus Fig. 2d), but the correlation is now negative ($r = -0.016$ with $p < 0.05$). We also consider links to ESM trends in the monthly EF values occurring on extreme days only (Supplementary Fig. 2). Then the correlation (Supplementary Fig. 2b versus Supplementary Fig. 2d) is $r = -0.113$ with $p < 0.05$. The mean of the simulated EF trends representing the recent past (Fig. 2d) shows more spatial consistency than ERA5-Land (Fig. 2c), likely in part due to averaging across a large set of models (similarly, comparing panels c and d in Supplementary Fig. 2).

We next consider if higher extreme temperature trends may instead link to increases in the mean H during the warmest half-year months (which is a diagnostic of the combined influence of change in available energy and evaporative fraction – see Introduction). We find that for ERA5-Land (Fig. 2e), there are some spatially consistent regions where extreme
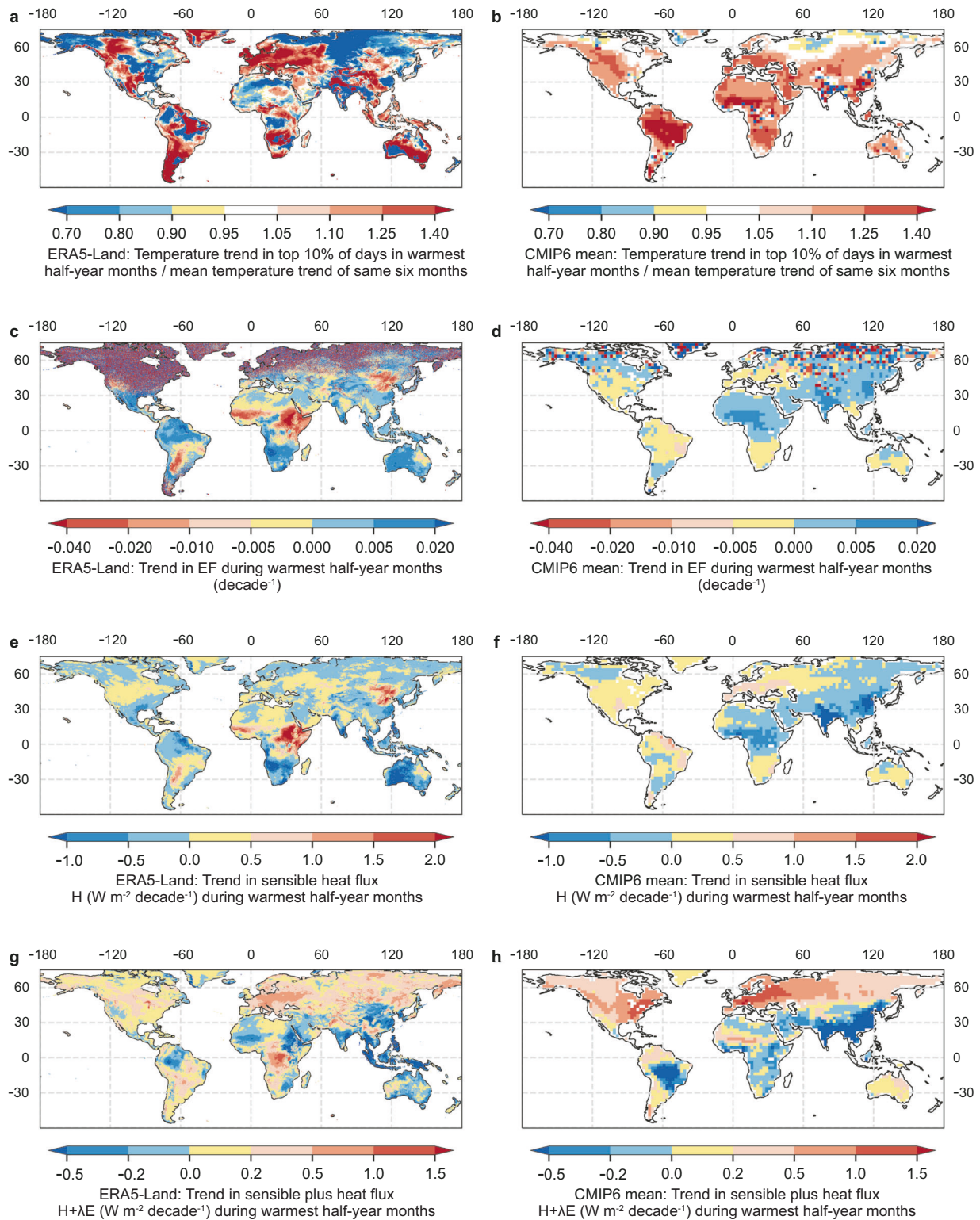
Fig. 2 | Maps of reanalysis and ESM-based temperature extreme acceleration and three potential energy-related covariates. a ERA5-Land-based trends in the warmest 10% of days in the warmest half-year months divided by trends of mean warming in the same 6 months. Values greater than unity represent an acceleration of extreme temperatures compared to mean warming trends in the same months. Calculated trends for years 1950 to 2021 inclusive on ERA5-Land gridboxes of 0.5° × 0.5° and for latitudinal range −60°S to 75°N. **b** Multi-ESM mean of, for each ESM, trends in the warmest 10% of warmest half-year month days divided by trends of mean warming in the same months, and hence the same variable as (**a**). Years used are also identical to (**a**). Calculations use the nearest ESM gridbox to midpoints of

common grid of 2.5° × 2.5°. Each point presented is where at least 30 of 32 ESMs have land-based data available and a land fraction cover of >95%. **c** is the trend in the mean evaporative fraction, EF, of the warmest half-year months, based on ERA5-Land data, for identical years and locations as (**a**) data. **d** is the multi-ESM mean of the individual trends for each ESM of mean EF during the warmest half-year months. These CMIP6-based trends use the same models, years and gridpoints as (**b**) data. **e** is of identical format to (**c**), except presenting ERA5-Land-based trends in H. **f** is identical to (**d**), except presenting the multi-ESM mean of trends in H. **g** is identical to (**c**), except it shows ERA5-Land-based trends in $H + \lambda E$. **h** is identical to (**d**), except it shows the multi-ESM mean of trends in $H + \lambda E$.

acceleration corresponds to positive trends in H, although overall, the correlation is slightly negative (Fig. 2e versus Fig. 2a; $r = -0.025$, $p < 0.05$). When considering trends in H on extreme temperature days only, the correlation becomes positive (Supplementary Fig. 2e versus Supplementary Fig. 2a; $r = 0.037$, $p < 0.05$). Similarly, for ESM projections over recent decades, there are distinct regions where more extreme warming coincides with positive H trends (Fig. 2f versus Fig. 2b; $r = 0.097$, $p < 0.05$). Notable is that when considering the trends in H for only months where extreme temperature days occur, there is a substantially higher positive correlation (Supplementary Fig. 2f versus Supplementary Fig. 2b; $r = 0.229$; $p < 0.05$).

For the mean of ESMs, although they project strong extreme temperature accelerations for parts of the tropics (Fig. 2b), the mean warmest half-year month trends in H are often negative (Fig. 2f). For this reason, we search for connections with extreme acceleration and trends in overall available surface energy, approximated as H plus λE (Fig. 2g for ERA5-Land and Fig. 2h for ESM projections). For calculations with ESMs, much of tropical Africa has positive trends in $H + \lambda E$, whereas H has a negative trend. Therefore, we create a masked area in the region of latitude 0.0 North to 30.0 North, where acceleration is greater than unity but sensible heat trends are negative. In this masked region, which includes much of Africa, we find a positive correlation between extreme acceleration and $H + \lambda E$ trends ($r = 0.129$, $p < 0.05$). Across non-masked points (in $-60°$S to $75°$N), the correlation between acceleration and trends in H becomes $r = 0.269$, $p < 0.05$. The equivalent statistics for the right column of Supplementary Fig. 2 are that for the masked region, the correlation between acceleration and $H + \lambda E$ is $r = 0.037$, $p < 0.05$, but in the non-masked area, the correlation with H reaches $r = 0.367$, $p < 0.05$. The suggestion here is that increases in sensible heat often relate to land drying and so a reduction in the fraction of available energy that is returned to the atmosphere as latent heat. However, in some locations, the overall available energy might not be invariant and increases, as approximated by positive trends in $H + \lambda E$ rise (despite declines in H). Without offering a rigorous explanation, this suggests that for places in our mask, there is a higher overall available energy at the land surface (e.g., due to altered future levels of cloud cover), which enhances temperature extremes.

As a sensitivity assessment, we check the robustness of spatial features of our extreme temperature acceleration findings using different forms of statistics, focusing on ERA5-Land data. In Supplementary Fig. 3a, we first reproduce Fig. 2a for comparison purposes. We then undertake a similar analysis but instead consider the trends in the warmest three months only and the trends in the top 10% of warmest days of those three months (Supplementary Fig. 3b). The values shown are again the ratio of the trends in extreme days divided by trends in the warmest (three) months. In general, there are strong similarities between Supplementary Fig. 3a and Supplementary Fig. 3b. Next, we constrain analyses to fixed sets of months, following the standard seasonal definitions, e.g., northern winter as December-February (DJF), and calculate the acceleration statistic for each three month period. Again, extremes considered are the top 10% of the highest daily temperatures, now for each three month period. In Supplementary Fig. 3c, if at least one season has an acceleration greater than unity, we present the season with the largest acceleration value. As may be expected, where acceleration is less than unity in warmest months (e.g., northern latitudes; Supplementary Fig. 3a, b), the largest accelerations are either not in JJA or there are no accelerations at all greater than unity (Supplementary Fig. 3c). In a final sensitivity test, we return to the warmest six (i.e., half-year) months and detrend their mean values. The linear regression coefficients associated with the detrending are used to further detrend the warmest 10% of days in those months. We study the resultant anomalies and derive their mean values for years 2000–2021 minus mean values for years 1950–1999. If this statistic is greater than zero, then the warmest extreme days are warming faster than the mean of the warmest half-year months. We show values of this statistic, which are in temperature units (Kelvin), in Supplementary Fig. 3d. Broadly, the regions of additional warming of extremes (Supplementary Fig. 3d) have similarities to accelerations greater than unity (Supplementary Fig. 3a).

Global analysis into the future

We also study the mean of ESM trends over a longer period, including the simulation of the decades ahead. Specifically, we determine the multi-ESM mean of trends projected for the period 1980–2079 (Fig. 3; quantities presented identical to the second column of Fig. 2, although trends are in the 41-year running means). We continue to show the ratio of temperature trends in the top 10% days of the 6 months of warmest background temperature versus the mean trends in the same 6 months (Fig. 3a; again, a value greater than unity corresponds to extreme temperature acceleration). Then, the following panels (Fig. 3b–d) show the mean trends, during the warmest half-year months, of EF, H and $H + \lambda E$, respectively. Values shown are for ESMs calculations with atmospheric GHG concentrations tracking their known historical values, followed by the SSP585 scenario[36]. These future-led calculations (Fig. 3) are for the same grid spacing as values derived for this historical period (Fig. 2, right column).

For the future (plus recent past) ESM-mean projections, the most noticeable feature of estimated extreme acceleration (Fig. 3a) is that the spatial spread shows less spatial variation compared to the historical period (Fig. 2b). The future projections estimate that almost all locations will experience the high-temperature extremes during the warmest half-year months rising faster than background warming in the same months, i.e., values greater than unity. Similar to the ESM projections for the historical period (Fig. 3a versus Fig. 2b), future warming acceleration is particularly high for Europe, much of South America and mid-USA. Projected ESM-mean future trends in mean EF during the warmest half-year months show local pattern consistency but strong regional variation, including differences in sign, and so low correlation with extreme temperature enhancement (Fig. 3b versus Fig. 3a; $r = -0.051$, $p < 0.05$). Supplementary Fig. 4 is identical to Fig. 3, except the diagrams are presented for modelled trends in energy fluxes only in the months of any daily extreme temperatures. The correlation between Supplementary Fig. 4b and Supplementary Fig. 4a is $r = -0.111$, although $p < 0.05$.

For much of the world, upward trends are simulated for future changes to sensible heat flux, H, with a relatively strong correlation of $r = 0.313$, $p < 0.05$ when comparing Fig. 3c versus Fig. 3a (reaching $r = 0.480$, $p < 0.05$ comparing Supplementary Fig. 4c versus Supplementary Fig. 4a). However, as for the contemporary period, an exception is a substantial fraction of Africa where there are negative trends in H (both Fig. 3c and Supplementary Fig. 4c). Hence, as for the contemporary period, we again create a masked area in the region of latitude 0.0 North to 30.0 North, and where temperature acceleration is greater than unity but sensible heat trends are negative. In this masked region, predominantly for Africa, we find a strong positive correlation between extreme acceleration and trends in $H + \lambda E$ (Fig. 3d) ($r = 0.526$, $p < 0.05$). In the remaining non-masked points, the correlation between acceleration and H (Fig. 3c) increases to $r = 0.479$, $p < 0.05$. When considering the trends in energy fluxes but only in the months of extremes (Supplementary Fig. 4c, d), the equivalent statistics are as follows. For the masked region, the correlation of trends in $H + \lambda E$ to acceleration falls to $r = 0.201$, $p < 0.05$, while in the non-masked areas, correlation with trends in H rises to $r = 0.556$, $p < 0.05$.

Discussion

There is a perception by much of society that the occurrence of extreme temperature events is increasing especially fast. Research has investigated whether the shape of the statistical distribution of daily temperatures is changing, and in particular, if the upper tail of the distribution is expanding such that high-temperature extremes are warming faster than mean temperatures. To analyse this, we calculate the warming trends of the hottest background 6 months (named "warmest half-year months"). Then, for the same 6 months, we estimate a second value of the warming trends in the hottest ten per cent of days of those months. Dividing the second value by the first gives a simple and intuitive statistic, which, if greater than unity, implies an additional rise in extreme temperatures compared to background warming of the warmest months i.e., an "acceleration" of extremes. Our analysis, therefore, focuses on shorter-term extreme events of order days up
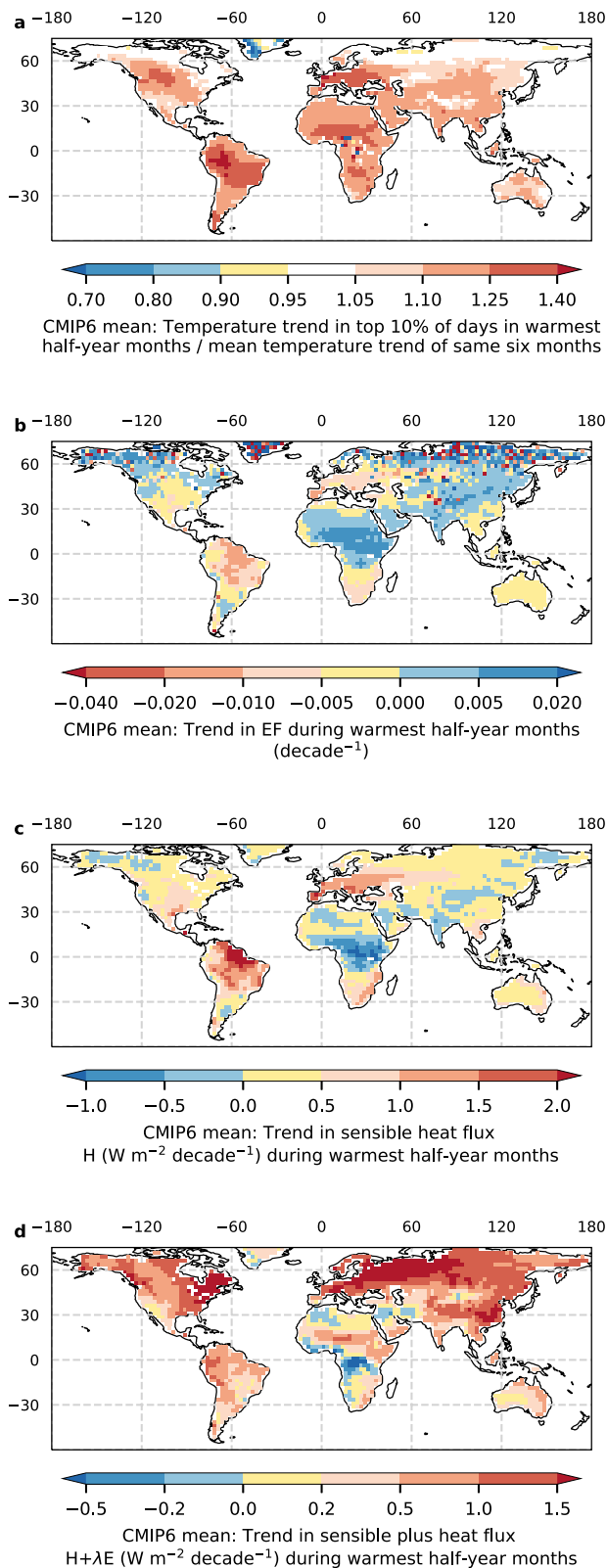
Fig. 3 | Projections by earth system models. Identical calculations to the right column of Fig. 2, except derived for the simulated period 1980–2079. **a** Multi-ESM mean of ESM-specific trends in the warmest 10% of days in warmest half-year months divided by trends of mean warming in same months. **b–d** Trends in mean values of EF, H and $H + \lambda E$, respectively, during the warmest half-year months. In one difference to Fig. 2, the trends are based on annual calculations of 41-year running means, with values centred on the years 1980–2079. The colourbar scales are identical to those of Fig. 2 to enable comparison.

to a couple of weeks, recognising that there are also concerns with changes to the frequency of longer monthly-timescale heatwaves (e.g., ref. 42). We note, developed in parallel, is the use of a similar ratio[6], applied to Europe and identifying higher warming rates of extremes there. Specific to the UK, (ref. 43) states in their executive summary that "UK extremes of temperature are changing much faster than the average temperature".

We find that for most land points, and for both the historical and future period forced by a high emissions scenario, the mean of ESMs predicts the acceleration ratio to be higher than unity. Values are typically an extra 20%, and while important to impact assessments, arguably, this is a level of acceleration that is neither very small nor very large. These values may explain why authors reach different conclusions that some extremes are accelerating[8] or, in general, their distribution is invariant except for an offset of background warming[9]. Importantly, when deriving the same ratio from the ECMWF ERA5-Land reanalysis product, there is much less geographical consistency than mean ESM projections for the recent past. Substantial spatial variation in features of high-temperature events may also cause authors to reach different conclusions on whether acceleration is occurring.

ERA5-Land entrains climatological data and should provide the most accurate statistics for recent daily temperature. If the geographically heterogeneous acceleration trends seen in the ERA5-Land product continue, adaptation planning for high-temperature extremes requires targeting specific locations. Fundamental questions relate to these discovered ERA5-Land versus ESM differences. Is the more homogenous extreme acceleration calculated in inter-ESM means a consequence of such averaging, whereas ERA5-Land represents only one realisation of the climate system? Is there something specific about recent decadal variations of the climate system captured by ERA5-Land that ESMs may emulate but not the specific timing? Atmospheric temperatures are known to be affected strongly by a range of decadal fluctuations in internal components of the Earth system (e.g., ref. 44), and related modes of circulation patterns impact regional extremes[45]. Relevant here is that efforts in decadal forecasting of extremes have high skill when extremes change faster than the mean[46]. Aerosols affect regional temperatures (e.g., ref. 47), and so also applicable here is a review of their modulation of extremes[48]. Assessment of aerosols on ECMWF reanalysis estimates of surface solar radiation is ongoing (e.g., for China, ref. 49). With evidence of extreme acceleration related to surface fluxes, ERA5-Land predictions of the latter will depend on its land surface module, H-TESSEL[50]. Assessment of biases in H-TESSEL and their role in estimating surface temperature (e.g., for specific regions[51]) and surface energy partitioning[52] is also continuing. Additional to the areal-mean of inter-ESM mean acceleration values being higher than that of ERA5-Land (spatial average of Fig. 2b versus 2a), we note again that the areal-means of individual ESMs, and for their simulations of the recent past, are also in general higher. That is, 29 of 32 ESMs (Supplementary Table 1) have a higher average extreme temperature acceleration than the value for ERA5-Land. Understanding these differences between ERA5-Land and ESMs is worthy of detailed investigation.

We present maps illustrating potential links between the acceleration of high temperature extremes during the warmest half-year months and mean trends in land-atmosphere energy fluxes during such months. Our highest correlation statistics between ESM projections of future acceleration ratio value and trends in the monthly mean values of sensible heat on the days of temperature extremes, but when excluding some tropical regions. In our excluded tropical locations, which in particular include parts of Africa, we instead find strong correlations with extreme temperature acceleration and trends in available energy. Existing research relates the adjustment of surface energy fluxes to altered soil drying (see Introduction and references therein). Others make such links through more sophisticated descriptions of drought, involving precipitation and potential evapotranspiration, and their feedback on high-temperature events[53]. In that context ref. 54 notes that understanding compound drought and high-temperature events requires a reduction of uncertainty in ESM estimates of future rainfall trends[55]. Emerging are reviews that provide a detailed process understanding of

heatwaves, including drivers and feedbacks[56]. That review[56] discusses regional-to-local factors and specifically references how drier soils enhance heatwave strength via modulated surface energy partitioning.

As knowledge advances, we hope our analysis provides a strong incentive to discover mechanisms that relate the values of our intuitive ratio of high-temperature acceleration to changing components of the Earth system. Boreal land regions are known to have warmed particularly fast in recent decades, which is likely due to earlier snowmelt and altered levels of evaporation adding to background warming. Research may help illustrate if such processes are impacting heatwaves less, causing the lower-than-unity extreme temperature accelerations for these regions. While we have searched for features of land energy fluxes impacting heat extreme attributes, the discussion of ref. 57 reiterates that high temperature events may often be linked to atmospheric dynamics as well as land-atmosphere feedbacks. A study[58] of the impact of land-atmosphere feedbacks on hot extremes in China uses two versions of the Weather Research and Forecasting (WRF) model, one of which is the standard configuration and the second with the interactive soil component replaced with inter-year mean conditions. That analysis illustrates how soil moisture conditions can impact high temperature extremes but it also noted other factors, such as Sea Surface Temperature (SST) anomalies, also have an important role via atmospheric connections. An analysis of extremes in the U.S. Midwest[59] finds that atmospheric anomalies play a significant role in summer drought events, and their contribution is less uncertain between atmospheric models than the influence of simulated land-atmosphere coupling. We have also not considered how changes in vegetation impact droughts. For instance, increased growth in warmer and CO_2-enriched climate may lead to greater evaporation and soil moisture loss[60]. In addition to explaining the acceleration of temperature extremes in many regions, a better understanding of contemporary data may allow for the ranking of predictive capability of ESMs. A detailed follow-up analysis of individual ESMs may be beneficial to determine if they exhibit greater regional heterogeneity of acceleration than that observed in the mean of ESMs, and which models are most consistent with ERA5-Land data. Temporal analysis of ESMs may reveal the extent to which levels of extreme acceleration and any correlations with surface energy fluxes are independent of the level of background climate change. Examining ESM simulations that exist forced with other SSPs may offer evidence that our acceleration ratio is independent of the trajectory of climate change.

Much recently observed global warming is attributable to burning fossil fuels, e.g., ref. 61, and including increasing regional temperatures[62]. With such warming, the frequency of extreme temperatures has also increased[63], also formally attributed to human influence[64]. Climate change is already impacting human health through multiple mechanisms, including heatwaves[65], and the seriousness of such events is reflected by a chapter of the latest IPCC report[66] reserved for extreme analysis[67]. Extreme high-temperature events often result from complicated connections between different components of the climate system, as illustrated by analyses of individual heatwaves (e.g., ref. 68). Critically, there is a perception that high temperatures are "running away" beyond general background global warming levels. Therefore, we have developed our ratio of extreme acceleration statistic, here for the top 10% of warmest days in the warmest half-year months. We note a recent attempt to place upper bounds on the magnitude of high-temperature events[69].

Our overarching finding is that except for very high northern latitudes, ESMs project ongoing and future extreme temperature acceleration beyond background warming levels during the hottest months. ERA5-Land also estimate historical warming acceleration but it is not as geographically universal as seen in ESM simulations. Given the high societal concern related to an increased frequency of very high-temperature events, these differences require examination. An investigation of reanalysis versus ESM differences may reveal if there remains an incomplete process parameterisation in ERA5-Land, or a broad deficiency in ESMs requiring correction to prevent any overestimation of increases in extreme temperatures. Although we can only as yet provide limited process insights, we hope our

intuitive ratio statistic will act as a catalyst to develop a more robust understanding of expected future high-temperature events as GHGs rise and any links to evolving climate attributes such as land-atmosphere energy exchanges.

Methods
We build our analysis on two primary sources of information. The first is Earth System Models (ESMs), designed to project how the climate will evolve for prescribed levels of changing atmospheric greenhouse concentrations. ESMs (e.g., refs. 70,71) solve differential equations on numerical grids that simulate the physical attributes of the climate system, including the movement of heat in and between the atmosphere, oceans, land and cryosphere. The role of ESMs is to estimate how different levels of atmospheric GHGs adjust the balance between incoming and outgoing radiation, modulating such heat flows and including their impact on near-surface meteorology. To capture processes well and for computational stability, ESMs perform calculations at short numerical timesteps and so can provide outputs relevant to understanding the evolving risk of extreme weather events. The second information source is our use of the 5th version of the ECMWF (European Centre for Medium-Range Weather Forecasts) ReAnalysis product (ERA5) and, in particular, the enhanced component over land, ERA5-Land Land[40]. Reanalysis products provide a set of detailed weather "hindcasts" for all days of recent decades, enabling an assessment of recent climatological changes to extremes. Hence, ERA5-Land offers a comparison to ESM calculations of the historical period and their statistics of simulated high-temperature events. We give details on both data sources below.

Earth system models
We use the latest set of ESMs held in the CMIP6 (Coupled Model Intercomparison Project Phase 6) ensemble database[39] (https://esgf-node.llnl.gov/search/cmip6/)[72]. ESMs in the CMIP6 database are all designed to project changes to climate, including simulating future near-surface meteorological conditions for different potential scenarios of atmospheric Greenhouse Gas (GHG) concentrations. ESMs provide information on a geographical grid (which differs between models) and for a range of timesteps. Such timesteps of model outputs can be relatively small (i.e., sub-monthly), so ESMs can be used to project changes in the statistical structure of temperature extremes as atmospheric GHGs rise. Throughout our analysis, we concentrate on calculations corresponding to the Shared Socio-Economic SSP585 pathway[36–38], which is sometimes referred to as a "high emissions, business-as-usual" approach to GHG emissions. With much societal discussion on how to lower emissions and with the frequently stated aim to stabilise global warming at or below 1.5 °C or 2.0 °C above pre-industrial levels, our use of the SSP585 pathway may provide an outer bound on potential future changes to near-surface temperature.

For each ESM, we extract daily near-surface air temperature, usually defined as two metres above the ground, and given the standard name of 'tas' (K). This is available at all locations on the numerical grid of each ESM, and importantly for extremes, is calculated in all models at the daily timestep. To analyse the link between daily temperature statistics and land-atmosphere energy fluxes, we additionally extract values of surface upward sensible heat flux, H, ('hfss') (W m^{-2}) and surface upward latent heat flux, λE, ('hfls') (W m^{-2}). These energy fluxes are, however, generally only available at the monthly modelled timescale. Also extracted from each ESM is the mask of the fraction of land area for each gridbox ('sftlf').

We select our ESMs (Supplementary Table 1) based on their availability in the UK JASMIN repository of CMIP6 data and during 2022. To use a model, our three variables of tas, hfss and hfls must be available for both the simulated historical period and calculations corresponding to the SSP585 forcing scenario. Specifically, we retain an ESM if there is at least one continuous simulation through both periods, starting in the modelled year 1850 and operating to at least the year 2099. Model outputs must be complete through that period, i.e., available every day for temperature and every month for the surface energy fluxes. Many ESMs have more than one full

such simulation, and we adopt the first listed numerically, and this corresponds to the CMIP6 notation of either ensemble member "r1i1p1f1" or "r1i1p1f2" (except for the CESM2 model where the first available is "r4i1p1f1"). Although some ESMs have multiple simulations available, we select just one member so that each model has an equal influence on our analysis. In total, we study 32 ESMs that fulfil the criteria above, and these are listed in Supplementary Table 1.

ERA-5 land reanalysis data

As a proxy for data over recent decades and for comparison against historical projections by ESMs, we study calculations with a reanalysis-based product from the European Centre for Medium-range Weather Forecasts (ECMWF). Reanalyses combine archived weather-forecast-type model calculations with many different streams of climatological observations to create a form of best estimate of meteorological conditions on each day in recent decades. We use available data for the years 1950 to 2021 inclusive. We use the version of reanalysis calculations from the ERA5-Land database[40] (https://doi.org/10.24381/cds.e2161bac)[73]. Daily data is available for variables the ECMWF name as *t2m*, *sshf* and *slhf* for temperature, sensible heat and latent heat, respectively. These quantities are available on a 0.25° × 0.25° spatial grid.

Acceleration and land-atmosphere energy exchange statistics

The main paper provides general details of the derivation of the acceleration statistic based on temperature trends and trends in features of land-atmosphere energy exchanges. The very fine details of how these values are compiled from ESM and ERA5-Land data are provided in full and in a single text location in the Calculations section of Supplementary Information.

Data availability

ESM data for the CMIP6 Earth System Models analysed is from the Earth System Grid Federation at https://esgf-node.llnl.gov/search/cmip6/ although the particular files analysed were those mirrored on the JASMIN system, the data analysis facility for environmental science based in the UK (files accessed and downloaded for local analysis during mid-2022). ERA5-Land data is available through the C3S Climate Data Store at https://doi.org/10.24381/cds.e2161bac.

Code availability

The numerical codes leading to Figs. 1–3 are available for download at https://doi.org/10.6084/m9.figshare.25382416.

References

1. Meehl, G. A. & Tebaldi, C. More intense, more frequent, and longer lasting heat waves in the 21st century. *Science* **305**, 994–997 (2004).
2. Dosio, A., Mentaschi, L., Fischer, E. M. & Wyser, K. Extreme heat waves under 1.5 degrees C and 2 degrees C global warming. *Environ. Res. Lett.* **13**, 054006 (2018).
3. Allan, R. P. et al. in *Climate Change 2021: The Physical Science Basis. Contribution of Working Group I to the Sixth Assessment Report of the Intergovernmental Panel on Climate Change* (eds Masson-Delmotte, V. et al.) (Cambridge University Press, 2021).
4. Huntingford, C. & Mercado, L. M. High chance that current atmospheric greenhouse concentrations commit to warmings greater than 1.5 °C over land. *Sci. Rep.-UK* **6**, 30294 (2016).
5. Byrne, M. P. Amplified warming of extreme temperatures over tropical land. *Nat. Geosci.* **14**, 837–841 (2021).
6. Patterson, M. North-West Europe hottest days are warming twice as fast as mean summer days. *Geophys. Res. Lett.* **50**, e2023GL102757 (2023).
7. Rousi, E., Kornhuber, K., Beobide-Arsuaga, G., Luo, F. & Coumou, D. Accelerated western European heatwave trends linked to more-persistent double jets over Eurasia. *Nat. Commun.* **13**, 3851 (2022).
8. Berg, A. et al. Impact of soil moisture–atmosphere interactions on surface temperature distribution. *J. Clim.* **27**, 7976–7993 (2014).
9. Thompson, V. et al. The 2021 western North America heat wave among the most extreme events ever recorded globally. *Sci. Adv.* **8**, eabm6860 (2022).
10. Estrada, F., Perron, P. & Yamamoto, Y. Anthropogenic influence on extremes and risk hotspots. *Sci. Rep.-UK* **13**, 35 (2023).
11. Guo, Y. M. et al. Quantifying excess deaths related to heatwaves under climate change scenarios: A multicountry time series modelling study. *Plos Med.* **15**, e1002629 (2018).
12. Mitchell, D. et al. Attributing human mortality during extreme heat waves to anthropogenic climate change. *Environ. Res. Lett.* **11**, 074006 (2016).
13. Basu, R. & Samet, J. M. Relation between elevated ambient temperature and mortality: A review of the epidemiologic evidence. *Epidemiol. Rev.* **24**, 190–202 (2002).
14. Mora, C. et al. Global risk of deadly heat. *Nat. Clim. Change* **7**, 501 (2017). +.
15. Battisti, D. S. & Naylor, R. L. Historical warnings of future food insecurity with unprecedented seasonal heat. *Science* **323**, 240–244 (2009).
16. Vogel, E. et al. The effects of climate extremes on global agricultural yields. *Environ. Res. Lett.* **14**, 054010 (2019).
17. Reichstein, M. et al. Climate extremes and the carbon cycle. *Nature* **500**, 287–295 (2013).
18. Williams, I. N., Torn, M. S., Riley, W. J. & Wehner, M. F. Impacts of climate extremes on gross primary production under global warming. *Environ. Res. Lett.* **9**, 094011 (2014).
19. Jones, M. W. et al. Global and regional trends and drivers of fire under climate change. *Rev. Geophys.* **60**, e2020RG000726 (2022).
20. Nolan, R. H. et al. Limits to post-fire vegetation recovery under climate change. *Plant Cell Environ.* **44**, 3471–3489 (2021).
21. Horton, R. M., Mankin, J. S., Lesk, C., Coffel, E. & Raymond, C. A review of recent advances in research on extreme heat events. *Curr. Clim. Change Rep.* **2**, 242–259 (2016).
22. Eyring, V. et al. in *Climate Change 2021: The Physical Science Basis. Contribution of Working Group I to the Sixth Assessment Report of the Intergovernmental Panel on Climate Change* (eds Masson-Delmotte, V. et al.) (Cambridge University Press, 2021).
23. Miralles, D. G., Gentine, P., Seneviratne, S. I. & Teuling, A. J. Land-atmospheric feedbacks during droughts and heatwaves: state of the science and current challenges. *Ann. NY Acad. Sci.* **1436**, 19–35 (2019).
24. Dai, A. Drought under global warming: a review. *Wiley Interdiscip. Rev. Clim. Change* **2**, 45–65 (2011).
25. Dirmeyer, P. A., Balsamo, G., Blyth, E. M., Morrison, R. & Cooper, H. M. Land-atmosphere interactions exacerbated the drought and heatwave over Northern Europe during summer 2018. *AGU Adv.* **2**, e2020AV000283 (2021).
26. Fischer, E. M., Seneviratne, S. I., Luthi, D. & Schar, C. Contribution of land-atmosphere coupling to recent European summer heat waves. *Geophys. Res. Lett.* **34**, L06707 (2007).
27. Seneviratne, S. I. et al. Investigating soil moisture-climate interactions in a changing climate: a review. *Earth Sci. Rev.* **99**, 125–161 (2010).
28. Miralles, D. G., Teuling, A. J., van Heerwaarden, C. C. & de Arellano, J. V. G. Mega-heatwave temperatures due to combined soil desiccation and atmospheric heat accumulation. *Nat. Geosci.* **7**, 345–349 (2014).
29. Berg, A. et al. Land-atmosphere feedbacks amplify aridity increase over land under global warming. *Nat. Clim. Change* **6**, 869 (2016). +.
30. Whan, K. et al. Impact of soil moisture on extreme maximum temperatures in Europe. *Weather. Clim. Extrem.* **9**, 57–67 (2015).
31. Jaeger, E. B. & Seneviratne, S. I. Impact of soil moisture-atmosphere coupling on European climate extremes and trends in a regional climate model. *Clim. Dyn.* **36**, 1919–1939 (2011).

32. Kone, B. et al. Influence of initial soil moisture in a regional climate model study over West Africa—Part 2: impact on the climate extremes. *Hydrol. Earth Syst. Sci.* **26**, 731–754 (2022).

33. Ganeshi, N. G. et al. Soil moisture revamps the temperature extremes in a warming climate over India. *Npj Clim. Atmos. Sci.* **6**, 12 (2023).

34. Zhang, J. Y., Yang, Z. M., Wu, L. Y. & Yang, K. Summer high temperature extremes over Northeastern China predicted by spring soil moisture. *Sci. Rep.-UK* **9**, 12577 (2019).

35. Lian, X. et al. Summer soil drying exacerbated by earlier spring greening of northern vegetation. *Sci. Adv.* **6**, eaax0255 (2020).

36. O'Neill, B. C. et al. The scenario model intercomparison project (ScenarioMIP) for CMIP6. *Geosci. Model Dev.* **9**, 3461–3482 (2016).

37. O'Neill, B. C. et al. The roads ahead: narratives for shared socioeconomic pathways describing world futures in the 21st century. *Glob. Environ. Chang.* **42**, 169–180 (2017).

38. Meinshausen, M. et al. The shared socio-economic pathway (SSP) greenhouse gas concentrations and their extensions to 2500. *Geosci. Model Dev.* **13**, 3571–3605 (2020).

39. Eyring, V. et al. Overview of the Coupled Model Intercomparison Project Phase 6 (CMIP6) experimental design and organization. *Geosci. Model Dev.* **9**, 1937–1958 (2016).

40. Muñoz-Sabater, J. et al. ERA5-Land: a state-of-the-art global reanalysis dataset for land applications. *Earth Syst. Sci. Data* **13**, 4349–4383 (2021).

41. Stiegler, C., Johansson, M., Christensen, T. R., Mastepanov, M. & Lindroth, A. Tundra permafrost thaw causes significant shifts in energy partitioning. *Tellus B Chem. Phys. Meteorol.* **68**, 30467 (2016).

42. Cowan, T., Undorf, S., Hegerl, G. C., Harrington, L. J. & Otto, F. E. L. Present-day greenhouse gases could cause more frequent and longer Dust Bowl heatwaves. *Nat. Clim. Change* **10**, 505–510 (2020).

43. Kendon, M. et al. State of the UK Climate 2022. *Int. J. Climatol.* **43**, 1–82 (2023).

44. Dai, A. G., Fyfe, J. C., Xie, S. P. & Dai, X. G. Decadal modulation of global surface temperature by internal climate variability. *Nat. Clim. Change* **5**, 555 (2015). +.

45. Kenyon, J. & Hegerl, G. C. Influence of modes of climate variability on global temperature extremes. *J. Clim.* **21**, 3872–3889 (2008).

46. Eade, R., Hamilton, E., Smith, D. M., Graham, R. J. & Scaife, A. A. Forecasting the number of extreme daily events out to a decade ahead. *J. Geophys. Res. Atmos.* **117**, D21110 (2012).

47. Collins, W. J. et al. Global and regional temperature-change potentials for near-term climate forcers. *Atmos. Chem. Phys.* **13**, 2471–2485 (2013).

48. Wang, Z. et al. Roles of atmospheric aerosols in extreme meteorological events: a systematic review. *Curr. Pollut. Rep.* **8**, 177–188 (2022).

49. He, Y. Y., Wang, K. C. & Feng, F. Improvement of ERA5 over ERA-interim in simulating surface incident solar radiation throughout China. *J. Clim.* **34**, 3853–3867 (2021).

50. Balsamo, G. et al. A revised hydrology for the ECMWF model: verification from field site to terrestrial water storage and impact in the integrated forecast system. *J. Hydrometeorol.* **10**, 623–643 (2009).

51. Johannsen, F. et al. Cold bias of ERA5 summertime daily maximum land surface temperature over Iberian Peninsula. *Remote Sens. Basel* **11**, 2570 (2019).

52. Martens, B. et al. Evaluating the land-surface energy partitioning in ERA5. *Geosci. Model Dev.* **13**, 4159–4181 (2020).

53. Zhang, Q. et al. High sensitivity of compound drought and heatwave events to global warming in the future. *Earths Future* **10**, e2022EF002833 (2022).

54. Bevacqua, E., Zappa, G., Lehner, F. & Zscheischler, J. Precipitation trends determine future occurrences of compound hot–dry events. *Nat. Clim. Change* **12**, 350–355 (2022).

55. Lee, J. Y. et al. in *Climate Change 2021: The Physical Science Basis. Contribution of Working Group I to the Sixth Assessment Report of the Intergovernmental Panel on Climate Change* (eds Masson-Delmotte, V. et al.) 553–672 (Cambridge University Press, 2021).

56. Barriopedro, D., García-Herrera, R., Ordóñez, C., Miralles, D. G. & Salcedo-Sanz, S. Heat waves: physical understanding and scientific challenges. *Rev. Geophys.* **61**, e2022RG000780 (2023).

57. Zhou, S. et al. Land-atmosphere feedbacks exacerbate concurrent soil drought and atmospheric aridity. *Proc. Natl. Acad. Sci. USA* **116**, 18848–18853 (2019).

58. Zhang, J. Y. & Wu, L. Y. Land-atmosphere coupling amplifies hot extremes over China. *Chin. Sci. Bull.* **56**, 3328–3332 (2011).

59. Chen, L., Ford, T. W. & Swenson, E. The role of the circulation patterns in projected changes in spring and summer precipitation extremes in the U.S. Midwest. *J. Clim.* **36**, 1943–1956 (2023).

60. Zhang, Y., Keenan, T. F. & Zhou, S. Exacerbated drought impacts on global ecosystems due to structural overshoot. *Nat. Ecol. Evol.* **5**, 1490–1498 (2021).

61. Jones, G. S., Stott, P. A. & Christidis, N. Attribution of observed historical near-surface temperature variations to anthropogenic and natural causes using CMIP5 simulations. *J. Geophys. Res. Atmos.* **118**, 4001–4024 (2013).

62. Stott, P. A. Attribution of regional-scale temperature changes to anthropogenic and natural causes. *Geophys. Res. Lett.* **30**, 1728 (2003).

63. Donat, M. G. et al. Updated analyses of temperature and precipitation extreme indices since the beginning of the twentieth century: The HadEX2 dataset. *J. Geophys. Res. Atmos.* **118**, 2098–2118 (2013).

64. Engdaw, M. M., Steiner, A. K., Hegerl, G. C. & Ballinger, A. P. Attribution of observed changes in extreme temperatures to anthropogenic forcing using CMIP6 models. *Weather. Clim. Extrem.* **39**, 100548 (2023).

65. Patz, J. A., Campbell-Lendrum, D., Holloway, T. & Foley, J. A. Impact of regional climate change on human health. *Nature* **438**, 310–317 (2005).

66. IPCC. *Climate Change 2021: The Physical Science Basis. Contribution of Working Group I to the Sixth Assessment Report of the Intergovernmental Panel on Climate Change*. In Press (Cambridge University Press, 2021).

67. Seneviratne, S. I. et al. in *Climate Change 2021: The Physical Science Basis. Contribution of Working Group I to the Sixth Assessment Report of the Intergovernmental Panel on Climate Change* (eds Masson-Delmotte, V. et al.) 1513–1766 (Cambridge University Press, 2021).

68. Trenberth, K. E. & Fasullo, J. T. Climate extremes and climate change: the Russian heat wave and other climate extremes of 2010. *J. Geophys. Res. Atmos.* **117**, D17103 (2012).

69. Zhang, Y. & Boos, W. R. An upper bound for extreme temperatures over midlatitude land. *Proc. Natl Acad. Sci. USA* **120**, e2215278120 (2023).

70. Collins, W. J. et al. Development and evaluation of an Earth-System model-HadGEM2. *Geosci. Model Dev.* **4**, 1051–1075 (2011).

71. Seferian, R. et al. Evaluation of CNRM earth system model, CNRM-ESM2-1: role of earth system processes in present-day and future climate. *J. Adv. Model. Earth Syst.* **11**, 4182–4227 (2019).

72. CMIP6 data. https://esgf-node.llnl.gov/search/cmip6/ (Repository of the Earth System Grid Federation, ESGF).

73. ERA5-Land data. https://doi.org/10.24381/cds.e2161bac (Repository of the Climate Data Store, hosted by the European Union Copernicus Project).

Author contributions

C.H. developed the acceleration metric, undertook the analysis and created the display items. All authors contributed extensively to the discussion of the results and the final form of the diagrams. All authors supported the writing of the manuscript.

Competing interests

The authors declare no competing interests.

Additional information